

Efficacy of information transmission in cellular communication

Sumantra Sarkar*

*Center for Nonlinear Studies, Theoretical Division, Los Alamos National Laboratory, Los Alamos, New Mexico 87545, USA
and Department of Physics, Indian Institute of Science, Bangalore 560012, India*

Md Zufikar Ali†

Department of Systems Biology, University of Massachusetts Chan Medical School, Worcester, Massachusetts 01605, USA

Sandeep Choubey‡

*The Institute of Mathematical Sciences, CIT Campus, Taramani, Chennai 600113, India
and Homi Bhabha National Institute, Training School Complex, Anushaktinagar, Mumbai 400094, India*

(Received 19 October 2020; accepted 18 January 2023; published 9 February 2023)

Cell signaling is essential for individual cells to execute various tasks and respond to changes in their environment. It is carried out via diffusing molecules, whose transport is often aided by directional advection. How diffusion and advection together impact the accuracy of information transmission during signaling remains poorly understood. Here, we study this problem using a simplified model of signal transport in the presence and absence of crowding. Mutual information, our measure of accuracy, shows three distinct regimes characterized by power-law decay. Surprisingly, crowding has no measurable effect on information transmission. Our results provide several important insights into the role of transport in cell signaling.

DOI: [10.1103/PhysRevResearch.5.013092](https://doi.org/10.1103/PhysRevResearch.5.013092)**I. INTRODUCTION**

The ability of individual cells to communicate and correctly respond to any alteration in their environmental cues forms the basis of development, immunity, and tissue repair. During cellular communication, an individual cell receives signals from nearby cells or the surrounding environment. Upon receiving the external signal, the cell transmits the decoded information about the extracellular environment to downstream effectors, which enables the cell to regulate its physiological state in response to changing environments [see Fig. 1(a)]. Similarly, within a cell, various organelles communicate by transporting materials via molecular motors along cytoskeletal filaments. Examples of such cellular communication systems include pheromone diffusion, quorum sensing, ion channel (e.g., calcium) diffusion, molecular motors carrying cargo along microtubules, etc. [Fig. 1(a)] [1–4].

Cellular communication is carried out by diffusible signaling molecules [1]. Often the motion of such signaling molecules is aided by active processes that provide directional advection [1]. Motor proteins (such as kinesins, myosins, etc.)

carrying cargo are one such example. Hence cellular communication is essentially carried out via an interplay between passive and active transport of signaling molecules, which can impact their ability to reliably communicate. While the efficacy of cellular communication has been studied extensively using ideas from information theory [5–16], most of these studies focused on biochemical networks involved in the various signaling pathways [9,17–21]. Currently, there is a burgeoning interest in understanding how transport properties of signaling molecules impact the accuracy of information transmission [22–24]. To achieve this goal, the complex details of the biochemical pathways are abstracted out as featureless molecules that move between a transmitter and a receptor through drift and diffusion. In this paradigm of *molecular communication* [23], the key goal is to understand the accuracy of information transmission, such as through mutual information (MI), and engineer communication channels to improve the efficacy of information transmission. In this paper, our goal is to develop a theory for molecular communication that can help design better molecular communication channels. Hence, while the accuracy of information transmission involves both biochemical reactions and signal transport, here we focus on the latter. The goal of this paper is to develop a framework that allows us to study the efficacy of temporal information transmission during cellular communication.

II. MODEL

We consider a simple stochastic model of cellular communication (Fig. 1): Signaling molecules moving in a one-dimensional (1D) channel of length L . The transmitter

*sumantra@iisc.ac.in

†zulfikar.ali@umassmed.edu

‡sandeep@imsc.res.in

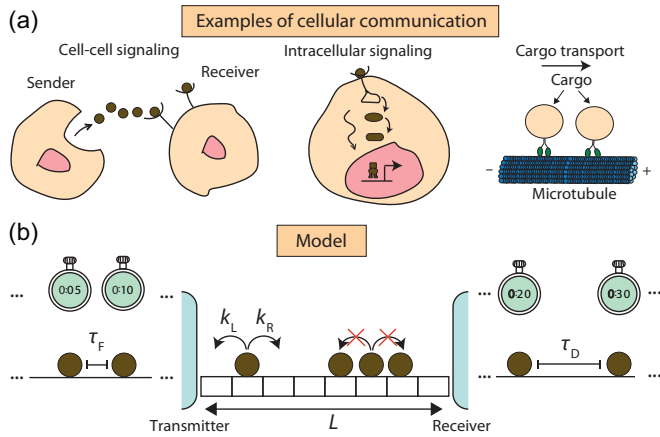


FIG. 1. Model of cellular communication: (a) Examples of cellular communication systems. (b) A simple 1D model of cellular communication channels. See text for details.

and receiver of the signal are located at $x = 0$ and $x = L$ [Fig. 1(b)], respectively. Once transmitted, each signaling molecule moves on a 1D lattice of lattice spacing a [Fig. 1(b)]. This translates to $N = L/a$ number of lattice sites in the channel. The transport of a molecule is characterized by two rates: The rate of hopping toward the receiver k_R and the rate of hopping toward the transmitter k_L . Each lattice site can be occupied by only one molecule. Consequently, owing to the excluded volume interaction, a signaling molecule can only hop toward an unoccupied neighboring site. After traversing the channel, a molecule is captured by the receiver at $x = L$. In addition, we assume that the transmitter is a perfect reflector and the receiver is a perfect absorber. Hence we impose reflecting boundary conditions at $x = 0$ and absorbing boundary conditions at $x = L$. Signaling molecules are fired at different time points from the transmitter. The time between two consecutive firing events is denoted as $\tau_F = t_F^{(i+1)} - t_F^{(i)}$. The time between consecutive detection events is given by $\tau_D = t_D^{(j+1)} - t_D^{(j)}$. Here, t_F^i and t_D^j denote the i th firing event and j th detection event. We assume that the receiver gathers information about τ_F from τ_D . Therefore the information processing by the communication channel is intertwined with the underlying transport process.

To characterize the impact of transport on the efficacy of information transmission, we compute the mutual information (a well-established metric to characterize information transmission [7]) between the firing time interval and the detection time interval:

$$I(\tau_F; \tau_D) = \sum_{\tau_F} \sum_{\tau_D} P(\tau_F, \tau_D) \log_2 \frac{P(\tau_F, \tau_D)}{P(\tau_F)P(\tau_D)} \quad (1)$$

$$= \sum_{\tau_F} \sum_{\tau_D} P(\tau_F)P(\tau_D|\tau_F) \log_2 \frac{P(\tau_D|\tau_F)}{P(\tau_D)}. \quad (2)$$

Here, $P(\tau_F)$, $P(\tau_D)$, and $P(\tau_F, \tau_D)$ are the probability distribution of the firing time interval, the probability distribution of the detection time interval, and the joint probability of firing and detection time, respectively. Furthermore, without any loss of generality, we define the normalized mutual

information,

$$I = \frac{I(\tau_F; \tau_D)}{H(\tau_F)}, \quad (3)$$

where $H(\tau_F)$ is the entropy of the firing time distribution. Using this characterization of information transmission, we explore two scenarios of our model: (1) in the absence of crowding, when the excluded volume interaction is not considered and (2) in the presence of crowding. In the first scenario, we obtain an analytical solution for the mutual information using Eqs. (2) and (3). The second scenario is biologically more realistic since it explicitly incorporates the effect of the excluded volume interaction; this is in line with various cellular communication processes as depicted in Fig. 1(a) [1]. In the ensuing section, we study the outcome of the two scenarios in detail. Surprisingly, we find that crowding has no measurable effect on information transmission.

III. INFORMATION TRANSMISSION IN THE ABSENCE OF CROWDING

To delineate the impact of the transport properties of signaling molecules on $I(\tau_F; \tau_D)$, first, we consider the scenario when the firing events are separated enough such that the influence of the excluded volume interaction is negligible. Under these conditions, we employ a continuum version of our model, whereby the transport process of signaling molecules is described by drift and diffusion. The rates of hopping (k_L and k_R) and lattice spacing can be used to determine the corresponding diffusion coefficient $D = a^2(k_R + k_L)/2$ and the drift velocity $v = a(k_R - k_L)$, respectively, in the limit $a \ll L$ [1] (see Appendix B for details).

We assume that in 1D, even in the absence of crowding, the ordering of firing events coincides with the ordering of detection events (see Appendix D). However, in dimensions higher than one dimension, the i th firing event may not lead to the i th detection event, as the i th signaling molecule may take a more circuitous path than the $(i + 1)$ th signaling molecule, ending up reaching the receiver later. We can write the detection times of two molecules, molecules 1 and 2, as

$$t_D^{(1)} = t_F^{(1)} + t_T^{(1)}, \quad (4)$$

$$t_D^{(2)} = t_F^{(2)} + t_T^{(2)}, \quad (5)$$

where $t_F^{(2)} > t_F^{(1)}$ and where $t_T^{(1,2)}$ are the transport times of the molecules. Because the receiver in our problem is a perfect absorber, the distribution of transport times is given by the first passage times of signaling molecules from the transmitter to the receiver, which we denote as $F(t)$. By combining Eqs. (4) and (5), we obtain

$$\tau_D = t_D^{(2)} - t_D^{(1)} = \tau_F + t_T^{(2)} - t_T^{(1)}. \quad (6)$$

To estimate the mutual information between τ_D and τ_F , we compute $P(\tau_D)$ and $P(\tau_D, \tau_F)$ in 1D using the following equations (Appendix A):

$$P(\tau_D) = \int_0^\infty d\tau_F \int_0^\infty dt P(\tau_F) F(t) F(\tau_F + t - \tau_D), \quad (7)$$

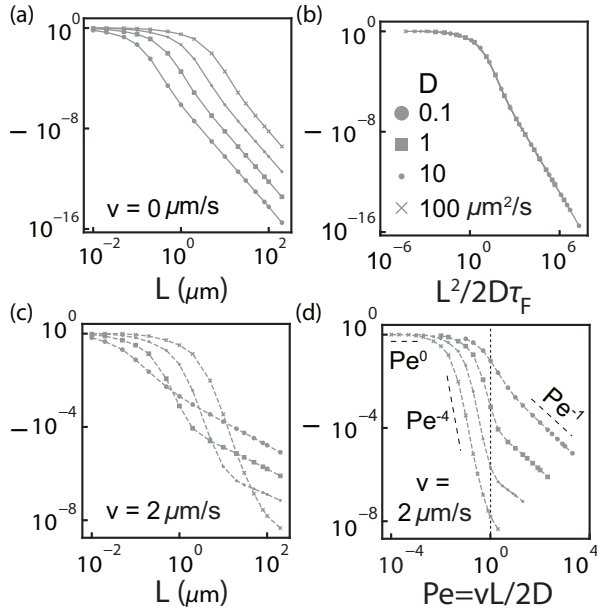


FIG. 2. Mutual information in the absence of crowding. (a) Normalized mutual information I as a function of channel length L for different diffusion coefficients [values shown in the legend of (b)]. (b) Normalized mutual information as a function of the ratio of transport time ($T = L^2/2D$) and firing time τ_F . (c) Normalized mutual information as a function of channel length in the presence of advection ($v = 2 \mu\text{m/s}$) for different D values, as shown in the legend of (b). (d) Normalized mutual information vs Péclet number ($Pe = vL/2D$) for different D values at $v = 2 \mu\text{m/s}$ showing distinct power-law behavior. $\tau_F = 0.01$ s was used to generate the figure.

$$P(\tau_D|\tau_F) = \int_0^\infty dt F(t)F(\tau_F + t - \tau_D) \quad (8)$$

$$= \int_0^\infty dt F(t)F(t - \Delta). \quad (9)$$

To the best of our knowledge, the first passage time distribution $F(t)$ is not known for the general system that we consider here. In the absence of crowding, we can obtain an analytical expression for $F(t)$ by solving the 1D diffusion equation, subject to appropriate boundary conditions. The solution yields an infinite series [25] that can be approximated by the closed-form expression given by

$$F(t) = \frac{CL}{\sqrt{4\pi Dt^3}} \exp\left[-\frac{(vt-L)^2}{4Dt}\right] \times \exp\left[-\frac{D^2 t^2}{2L^4}\right], \quad (10)$$

where C is a normalization constant. The functional form of $F(t)$ used here works well for all values of the drift velocity v (Appendix B).

Below, we use this expression of $F(t)$ to investigate how, in the absence of crowding, the interplay between advection and diffusion of signaling molecules affects mutual information between τ_F and τ_D . We assume τ_F to be exponentially distributed since it is the most natural choice for independent stochastic reactions.

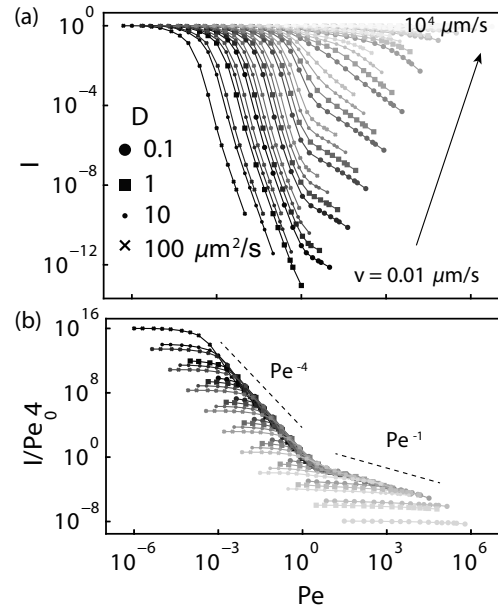


FIG. 3. Mutual information in the absence of crowding exhibits universal scaling. (a) Normalized mutual information I vs Péclet number (Pe) for different values of the drift velocities and diffusion coefficients (see legend). (b) Rescaled mutual information (I/Pe_0^4) vs Péclet number Pe collapse onto a single master curve that scales as Pe^{-4} for $Pe < 1$ and as Pe^{-1} for $Pe > 1$. $\tau_F = 0.01$ s is used to generate the figure.

A. Diffusive channels

In the absence of advection (when $v = 0$), transport happens purely through diffusion. For this setting, I depends on the channel length L and the diffusion coefficient D [Fig. 2(a)]. In general, we find that for a given value of D , I does not show any variation with the channel length L up to a D -dependent length scale, L_0 , beyond which I decays in a universal fashion across different diffusion coefficients. We find that L_0 corresponds to the channel length when the transport time T is comparable to the average time interval between consecutive firing events, $\langle\tau_F\rangle$, such that $L_0 \sim \sqrt{2D\langle\tau_F\rangle}$. We note that the transport time T is the average time to traverse a 1D channel of length L through diffusion and is given by $L^2/2D$. For $L > L_0$, we find that I is inversely proportional to the transport time T [Fig. 2(b)]. These observations suggest that the efficacy of information transmission undergoes a transition at the threshold L_0 : Below L_0 , mutual information is solely dictated by the firing time distribution $P(\tau_F)$ and remains unaffected by the transport process, whereas, above L_0 , diffusive transport determines the information transmission.

B. Advective channels

To explore the impact of nonzero driving, we compute the variation of I with L when $v > 0$. We observe that the transition at L_0 persists even in the presence of nonzero v [Fig. 2(c)]. Furthermore, the introduction of drift leads to another transition at another D -dependent characteristic length scale, L_1 . For $L > L_1$, I decays as L^{-1} , which is slower than the L^{-4} decay observed when $L_0 < L < L_1$. Since the L^{-4} dependence stems from the variation of the diffusive transport times with L , we suspect that the transition at L_1 originates from the

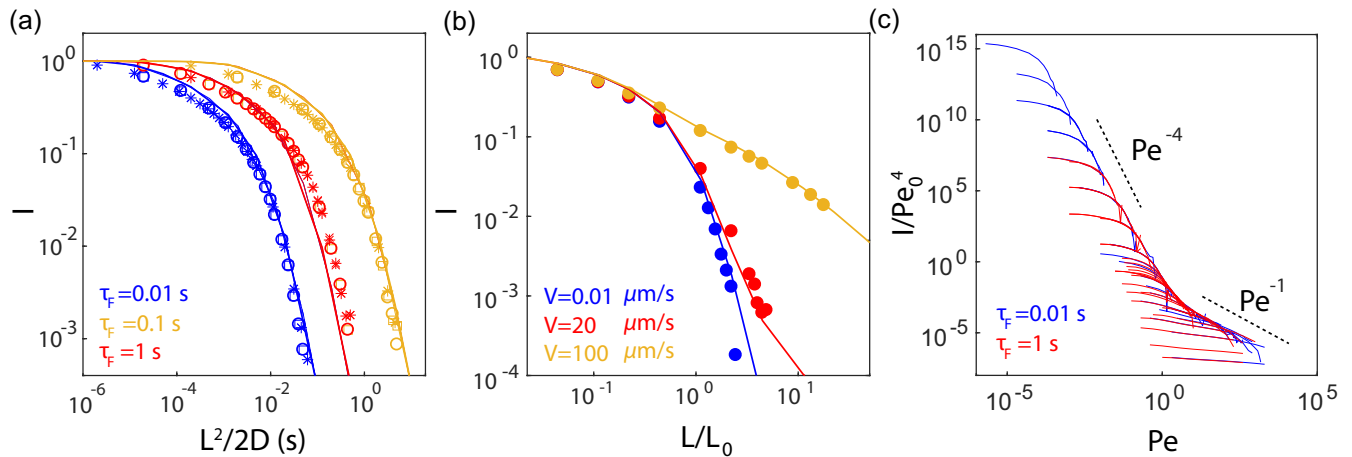


FIG. 4. Mutual information in the presence of crowding. (a) I vs $L^2/2D$ for $D = 0.1, 1, 10, 100 \mu\text{m}^2/\text{s}$ [symbols in Fig. 2(b)] and firing times ($\tau_F = 0.01, 0.1, 1$ s, colors) obtained from stochastic simulations. (b) I vs L/L_0 for $D = 10 \mu\text{m}^2/\text{s}$, $\tau_F = 0.01$ s, and $v = 0.01, 20, 100 \mu\text{m}/\text{s}$ (legend). The solid curves in (a) and (b) denote the prediction from theory in the absence of crowding. (c) I/Pe_0^4 vs Pe for $\tau_F = 0.01$ and 0.1 s (legend) shows identical scaling to that in the absence of crowding.

introduction of the advection. Indeed, when we compute I as a function of the Péclet number, $Pe = vL/2D$, we find that the transition to the L^{-1} (equivalently, Pe^{-1}) decay regime occurs precisely at $Pe = 1$, where the advection rate $vL/2$ is equal to the diffusion coefficient [Fig. 2(d)]. This observation also implies that $L_1 = 2D/v$. Interestingly, the variation of I with L (equivalently, with Pe) changes dramatically as v is changed over different values [Fig. 3(a)]. For smaller values of v , $Pe_{\max} = \max_L(Lv/2D)$ always stays below 1, whereas the opposite effect is seen for larger values of v . Furthermore, when I is scaled by $Pe_0^4 = (L_0v/2D)^4$, I versus Pe curves collapse onto a single master curve that scales as Pe^{-4} below $Pe < 1$ and as Pe^{-1} for $Pe > 1$ [Fig. 3(b)]. Such scaling is observed because, beyond L_0 , variation in MI is dictated by the transport process (Appendix E). In particular, we find that beyond this length scale, MI is inversely proportional to the variance of Δ , which shows exactly the same scaling behavior with Pe (Appendix E).

IV. MUTUAL INFORMATION IN THE PRESENCE OF CROWDING

In cellular systems and realistic molecular communication channels, the excluded volume interaction induced by crowding of the signaling molecules plays a central role in modulating their transport to the receiver [26]. To this end, we study the second scenario of our model, where the effect of crowding is considered. We employ stochastic simulations for the 1D model described in Fig. 1 using the Gillespie algorithm [27]. For the details of the simulation methodology, please see Ref. [28]. From the simulations, we obtain distributions of detection and firing time intervals. In general, computing the MI from samples of two random variables distributed according to some joint probability density is challenging [29]. To overcome this challenge, we use a state-of-the-art method given in Ref. [30] to compute the MI between arrival and detection time intervals, as obtained from simulations. In Fig. 4, we compare the results from simulations with analytical expressions obtained for the no-crowding scenario. MI in

the presence of crowding (see kymographs in Appendix C) overlaps with the no-crowding scenario and follows the same scaling behavior (see Fig. 4) for a wide range of parameter values. However, when the normalized MI falls below a certain threshold, of the order of $\sim 10^{-3}$ – 10^{-4} [see Figs. 4(a) and 4(b)], the method in Ref. [30] fails to compute MI reliably; the computed values of MI increasingly become noisier, often leading to negative values. It must be noted that the minimum sample size for the arrival and detection time intervals was chosen to be 10^5 , and an order-of-magnitude increase in the sample size did not significantly improve the accuracy of results. In addition, the findings do not depend on the choice of the lattice size (see Appendix C). Overall, for the observed range of parameter values, the presence or absence of crowding does not alter our findings.

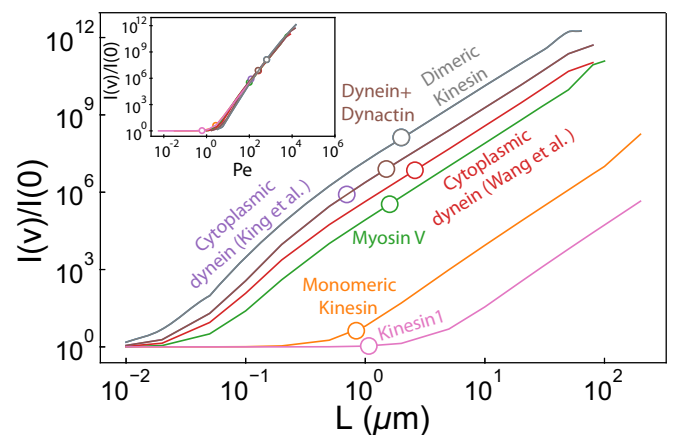


FIG. 5. $I(v)$ as a function of channel length L for advective channels normalized by $I(v = 0)$ for a diffusive channel ($v = 0$). Each curve corresponds to a molecular motor (monomeric and dimeric kinesin [31], dynein+dynactin [32], cytoplasmic dynein [32–34], myosin V [35], and kinesin-1 [36]), shown as data points in Table I. The inset shows $I(v = 0)/I(v = 0)$ as a function of the Péclet number. King *et al.*, King and Schroer [32]; Wang *et al.*, Wang and Sheetz [33].

V. DISCUSSION

In this paper, we study the effect of molecular transport on the efficacy of information transmission during cellular communication. Here, we study this problem using a simplified model of signal transport that involves an interplay between drift and diffusion in the presence and absence of crowding. For both scenarios, in a pure diffusive channel, MI exhibits a nonlinear decrease as a function of the channel length. Beyond a diffusion coefficient-dependent channel length L_0 , MI decreases sharply, exhibiting a power-law behavior. Notably, through a change in a variable, all the curves for mutual information as a function of transport time for a wide range of parameter values collapse onto a single master curve. The presence of crowding does not alter these findings within the observed range of parameter values. Note that we suspect that for a highly crowded channel, information transmission might be significantly impacted, leading to a sharper drop in MI compared with the no-crowding scenario. However, owing to the limitations of the existing methods [30] that compute MI from data, we cannot reliably probe this regime. When advection is added to the model, the MI initially remains constant for small values of the drift velocity; only at higher values does the MI increase substantially (see Appendix E) [23]. We discover that this effect can be characterized better when MI is plotted against the Péclet number: Only when $Pe > 1$ does drift improve the efficacy of information transmission. Interestingly, MI as a function of the Péclet number shows three distinct regimes with three different scaling factors. Our results demonstrate nontrivial dependence of information transmission on the transport properties of signaling molecules.

Here we must note that cellular communication systems often exhibit complex transport processes. For instance, motor protein transport might involve bidirectional motion, pausing along microtubule tracks, etc. [1]. Signaling can also involve carriers of different sizes and properties (ions, molecule-packed vesicles, etc.) [37]. Moreover, the cellular environment is crowded, and actively driven [38], leading to anomalous diffusion of signaling molecules [39]. While such complexities will impact the efficacy of information transmission, our results provide the necessary foundation to interpret more complicated models that consider these aforementioned facets of signal transport.

A renewed look into biological systems in light of these results provides interesting insights. For information transmission through molecular motors such as dynein [32,33], the Péclet number is above 1, signifying the importance of drift in improving the efficacy of information transmission (Fig. 5).

In contrast, for a couple of members of the kinesin family of motor proteins such as monomeric kinesin [31] and kinesin-1 [36], the reported drift velocities are inadequate in improving the efficacy of communication. Note that Fig. 5 serves as a proof of concept and does not capture cargo transport in cells. Cargo transport is a more complicated process and involves the assembly of multiple motor proteins. Studying the efficacy of cargo transport would entail a more detailed model that incorporates this assembly of motor proteins.

Since information transmission is a fundamental function of cellular communication networks, an exciting plausibility is that evolutionary pressures would shape the cellular machinery to maximize the reliable decoding of temporal signals.

ACKNOWLEDGMENTS

The authors thank S. Redner, J. Kondev, A. E. Garcia, and A. Narayanan for useful comments and critical reading of the manuscript. S.S. was funded by LDRD Grant No. (XX01) from LANL. This paper has the following report number: LA-UR No. LA-UR-20-28073. S.C. thanks MPI-PKS, Dresden, where a part of the work was done. S.C. is supported by the Ramalingaswami Re-entry Fellowship (BT/HRD/35/02/2006), a re-entry scheme of the Department of Biotechnology, Ministry of Science & Technology, Government of India.

APPENDIX A: DERIVATION OF THE PROBABILITY DISTRIBUTION OF τ_D

As shown in Eq. (6) in the main text, we have

$$\tau_D = \tau_F + t_T^{(2)} - t_T^{(1)}. \quad (\text{A1})$$

Here, $t_T^{(1)}$ and $t_T^{(2)}$ are the first passage times of two consecutive detection events, respectively, and τ_F is the interval between the corresponding firing events. Because τ_D is a function of these independent variables, its probability distribution can be estimated from the probability distribution of the independent variables. Namely,

$$\begin{aligned} P(\tau_D) &= \int_0^\infty d\tau_F P(\tau_F) \int_0^\infty dt_T^{(2)} F(t_T^{(2)}) \int_0^\infty dt_T^{(1)} F(t_T^{(1)}) \\ &\quad \times \delta(\tau_D - \tau_F - t_T^{(2)} + t_T^{(1)}) \\ &= \int_0^\infty d\tau_F P(\tau_F) \int_0^\infty dt_T^{(2)} F(t_T^{(2)}) F(\tau_F - \tau_D + t_T^{(2)}) \end{aligned} \quad (\text{A2})$$

$$(\text{A3})$$

TABLE I. Diffusion and advection values for molecular motors.

Molecular motor	v ($\mu\text{m/s}$)	D ($\mu\text{m}^2/\text{s}$)	L (μm)	Ref.
Monomeric kinesin	0.14	0.044	0.84	[31]
Dimeric kinesin	0.71	0.0022	2	[31]
Dynein+dynactin	0.7	0.0041	1.5	[32]
Cytoplasmic dynein	0.422	0.0041	2.6	[32–34]
Cytoplasmic dynein	0.7	0.0041	0.7	[32–34]
Myosin V	0.36	0.0058	1.6	[35]
Kinesin-1	0.8	1.4	1.07	[36]

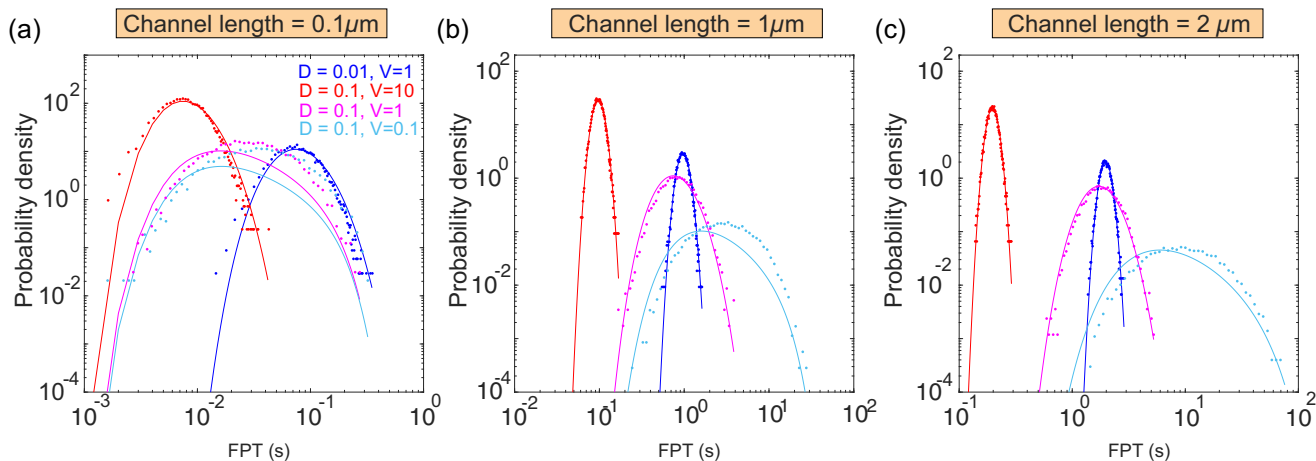


FIG. 6. First passage time (FPT) distribution obtained from a stochastic model without excluded volume interaction (dots) and Eq. (B3) (solid curves) for channel lengths (a) $L = 0.1 \mu\text{m}$, (b) $L = 1 \mu\text{m}$, and (c) $L = 2 \mu\text{m}$.

$$\begin{aligned}
 &= \int_0^\infty d\tau_F P(\tau_F) \\
 &\quad \times \int_0^\infty dt F(t) F(\tau_F - \tau_D + t) \text{ (write } t_T^{(2)} \rightarrow t)
 \end{aligned}
 \tag{A4}$$

$$\equiv \int_0^\infty d\tau_F P(\tau_F) P(\tau_D | \tau_F).
 \tag{A5}$$

APPENDIX B: FIRST PASSAGE TIME DISTRIBUTION

We model a cellular communication channel as a 1D finite region of length L with reflecting boundary condition at $x = 0$ and absorbing boundary condition at $x = L$. This setup is referred to as the transmission mode in Ref. [25]. The first passage time distribution for this problem is given by the first passage time distribution for free diffusion in infinite space added to the contribution from infinite image charges originating from the reflecting and the absorbing boundary conditions, resulting in an infinite sum of terms [25].

To avoid convergence issues of the infinite series during numerical evaluation, we use an approximate formula for the first passage time distribution. To construct this formula, we note that in the presence of a large enough drift in the $+x$ direction, the presence of the reflecting boundary is rarely felt by the transported molecule. Therefore the first passage time distribution is chosen to be of the following form:

$$F(t) = F_{\text{abs}}(t) * g(t),
 \tag{B1}$$

$$F_{\text{abs}}(t) = \frac{L}{\sqrt{4\pi Dt^3}} \exp\left[-\frac{(vt - L)^2}{4Dt}\right],
 \tag{B2}$$

where F_{abs} is the first passage distribution of a molecule transported in a semi-infinite line with the absorbing boundary condition at $x = L$ [23,25] and $g(t)$ is a function that captures the contribution of the reflecting boundary condition at $x = L$.

To determine $g(t)$, we simulate a 1D lattice model of length L with the same boundary condition. In the lattice model, the particle hops with a constant rate p in the $+x$ direction and with a rate q in the $-x$ direction. When $p = q$, the particle motion is purely diffusive, and when p and q are unequal, the

particle moves using both advection and diffusion. When $p > q$, the particle has an effective drift velocity of $a(p - q)$, where a is the length of each lattice site. The corresponding diffusion coefficient is $D = a^2(p + q)/2$ [1]. From the simulations, the measured first passage time distribution has a Gaussian tail (Fig. 6), and we find that the following ansatz approximates the true distribution well:

$$F(t) = \frac{CL}{\sqrt{4\pi Dt^3}} \exp\left[-\frac{(vt - L)^2}{4Dt}\right] \times \exp\left[-\frac{D^2 t^2}{2L^4}\right],
 \tag{B3}$$

where C is a normalization constant. We use this approximate formula because the first two moments of the distribution are nearly identical to the true distribution [25]. In fact, this ansatz was motivated by the analytical expressions of the first two moments derived in Ref. [25]. This result implies that $g(t) = \exp[-\frac{D^2 t^2}{2L^4}]$. To measure the first passage distribution using the lattice model, we generated 10 000 trajectories at each p value ($q = 1 - p$). As Fig. 6 shows, this approxima-

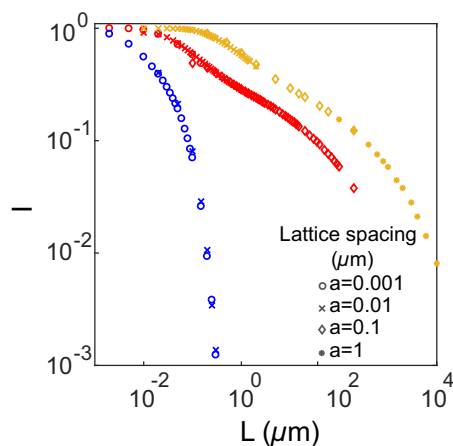


FIG. 7. Effect of lattice size on normalized MI. Data points obtained using different lattice sizes, $a = 0.001, 0.01, 0.1, 1 \mu\text{m}$ fall on a single curve for given D and v values: $D = 0.1 \mu\text{m}^2/\text{s}$, $v = 0$ (blue); $D = 1 \mu\text{m}^2/\text{s}$, $v = 10 \mu\text{m}/\text{s}$ (red); $D = 100 \mu\text{m}^2/\text{s}$, $v = 100 \mu\text{m}/\text{s}$ (yellow).

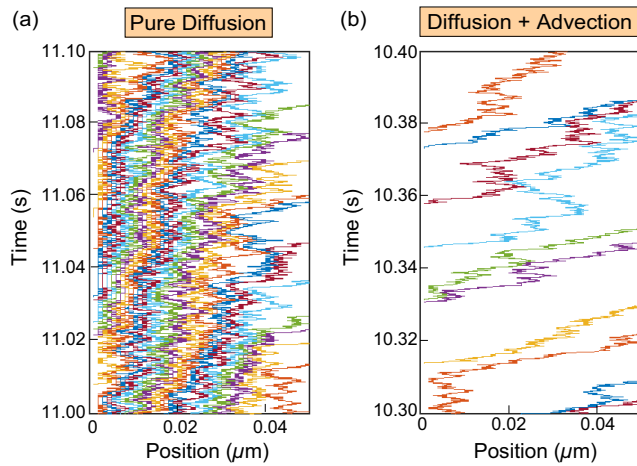


FIG. 8. Kymographs from stochastic simulations. Kymographs showing the clustering of signaling molecules for pure diffusion (a) and diffusion with advection (b). Different colors indicate molecules fired at different time points. The following parameters were used to generate the figure: $D = 0.1 \mu\text{m}^2/\text{s}$, $v = 0 \mu\text{m}/\text{s}$, $\tau_F = 0.01 \text{ s}$, and $L = 0.05 \mu\text{m}$ for (a); $D = 0.1 \mu\text{m}^2/\text{s}$, $v = 2 \mu\text{m}/\text{s}$, $\tau_F = 0.01 \text{ s}$, and $L = 0.05 \mu\text{m}$ for (b).

tion works quite well (the Péclet number varies from 0 to 4×10^2).

APPENDIX C: SIMULATION METHODOLOGY

We implement the Gillespie algorithm for stochastic reaction systems to compute the mutual information in a simple stochastic model of cellular communication. For this, we assume that the signaling molecules are moving in a one-dimensional channel of length L of lattice spacing a . This translates to $N = L/a$ number of lattice sites in the channel.

The transmitter and receiver of the signal are located at the first site ($x = 0$) and the last site ($x = L$), respectively. Signaling molecules are loaded at the first site at a rate k_{firing} only when unoccupied. Once loaded, each signaling molecule moves on a 1D lattice of lattice spacing a [Fig. 1(b) and Sec. II]. The transport of a molecule is characterized by two rates; the rate of hopping toward the receiver k_R and the rate of hopping toward the transmitter k_L . Each lattice site can be occupied by only one molecule. Consequently, owing to the excluded volume interaction, a signaling molecule can only hop toward an unoccupied neighboring site (the hopping rates are zero if there is a molecule in the vicinity). After traversing the channel, a molecule is captured by the receiver at $x = L$ and removed from the lattice. We also impose the condition that at the first lattice site, the signaling molecules can only move forward and cannot escape by traversing in a reverse direction. Both the firing time, i.e., the time of loading of signaling molecules at the first site, and the time of detection are recorded for at least 5×10^4 firing events (we skip the first 5000 events to get rid of the transient behavior); these data are then used to compute the mutual information between the firing time interval and the detection time interval. Note that variation in lattice spacing doesn't affect our findings, as shown in Fig. 7. Although the kymographs in Fig. 8 demonstrate that crowding dominates the dynamics of transport in the channel, the scaling behavior remains unaltered.

APPENDIX D: LIMITATIONS OF THE MODEL

We consider a simplified model of cellular communication using a one-dimensional channel. While our model provides key insights into the impact of signal transport on information transmission, there are important limitations that need to be mentioned. First, many realistic channels of communication in biology would involve two- and three-dimensional

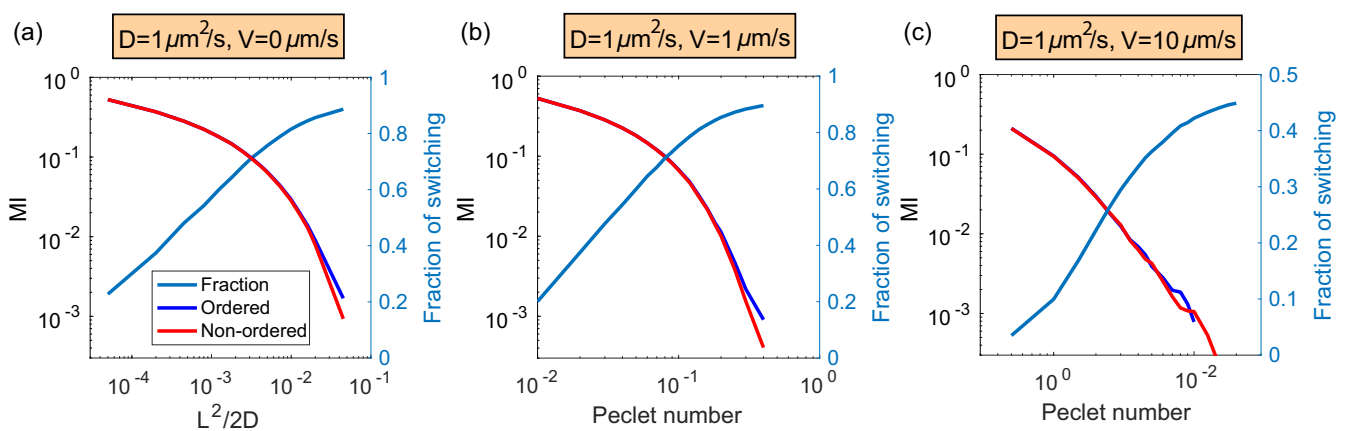


FIG. 9. (a)–(c) Stochastic simulation to tackle the ordering of signaling molecules during detection. Assuming that the signaling molecules are indistinguishable from each other, we order the signaling molecules based on their detection times. Hence for the i th firing event, multiple molecules corresponding to the $(i + n)$ th firing event (n is a positive integer) can be detected earlier. The blue and red curves represent MI computed using ordered and nonordered detection of signaling molecules. We observe how the scaling behavior of MI changes as the alteration in the order of detection events (fraction of switching) increases. Fraction of switching is defined as the fraction of events where order of detection between two consecutive firing events is switched (in cerulean blue). While we observe a small deviation for values of MI of less than $\sim 10^{-3}$, the overall nature and the scaling behavior do not change much. Moreover, deviations can be seen when the fraction of order switching between signaling molecules is more than 0.8.

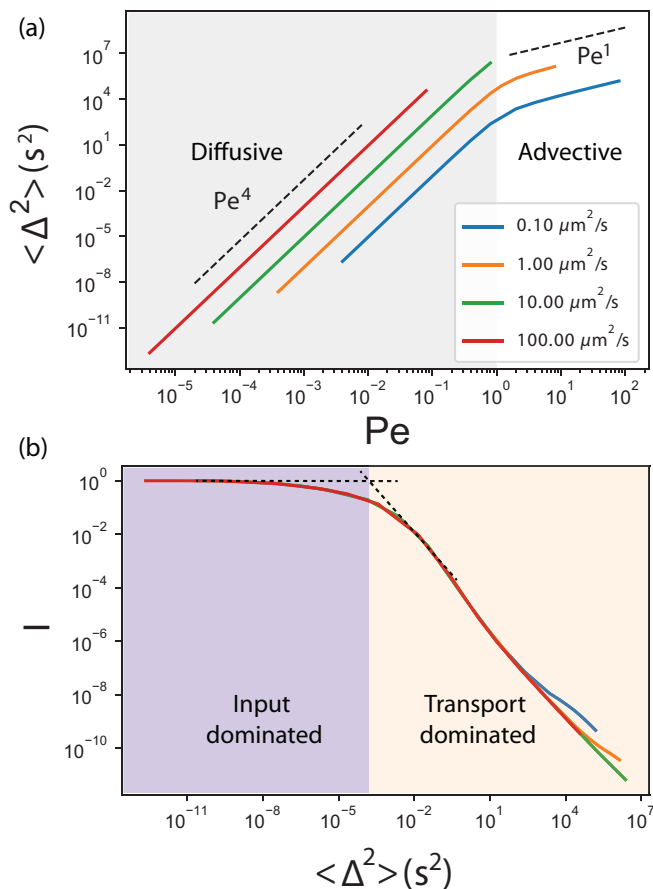


FIG. 10. (a) $\langle \Delta^2 \rangle$ vs Pe for different values of diffusion coefficients (legend) at drift velocity $v = 0.05 \mu\text{m/s}$. (b) I vs $\langle \Delta^2 \rangle$, showing that when $\langle \Delta \rangle \gg \langle \tau_F^2 \rangle = 10^{-4}$, I is inversely proportional to $\langle \Delta^2 \rangle$. The plots are generated using analytical expressions for the no-crowding scenario.

transport. While the insights gained from our model will definitely allow for a better understanding of the results corresponding to higher-dimensional communication channels, we suspect that our model cannot fully capture the behavior of higher-dimensional models. Second, our model assumes a fully reflecting boundary condition at the channel entrance and a fully absorbing boundary condition at the exit. For some channels, it is possible that the entrance is only partially reflecting. This might affect our findings. However, to the

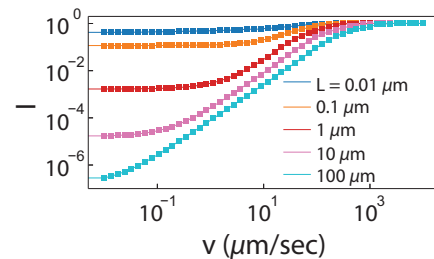


FIG. 11. Normalized MI as a function of drift velocity for different channel lengths. The diffusion coefficient is $D = 1 \mu\text{m}^2/\text{s}$. The plots are generated using analytical expressions for the no-crowding scenario.

best of our knowledge, for most of the channels in molecular or cellular communication, signaling molecules do not move back into the transmitter [1]. For a concrete example, consider cargo transport on a microtubule; most cargoes do not exit via the channel entrance. Our model assumptions are motivated by such systems. Third, we assume that in 1D, the ordering of firing events is preserved during detection, even in the absence of crowding. It is important to that a relaxation of this assumption does not alter the key findings (see Fig. 9).

APPENDIX E: RELATION BETWEEN TRANSPORT TIME AND MUTUAL INFORMATION

As shown in Sec. III, the time interval between two consecutive detection events is given by

$$\tau_D = t_D^{(2)} - t_D^{(1)} = \tau_F + t_T^{(2)} - t_T^{(1)}, \quad (\text{E1})$$

$$\tau_D = \tau_F + \Delta, \quad (\text{E2})$$

where Δ is the difference between the transport time of two consecutive molecules detected at the receiver. As Fig. 10(a) shows, the mean squared transport time difference $\langle \Delta^2 \rangle$ scales as Pe^4 when $\text{Pe} < 1$ and as Pe^1 for $\text{Pe} > 1$. This scaling is exactly the inverse of how I varies with Pe in Fig. 3, which implies that I is inversely proportional to $\langle \Delta^2 \rangle$. Indeed, as Eq. (E2) suggests, when $\tau_F \gg \Delta$, τ_D is determined by the firing time interval distribution τ_F (the input distribution). On the other hand, when $\Delta \gg \tau_F$, τ_D is determined by the transport process [Fig. 10(b)]. It must be noted that advection has a nonlinear effect on MI, as shown in Fig. 11.

[1] R. Phillips, J. Kondev, J. Theriot, and H. Garcia, *Physical Biology of the Cell* (Garland Science, London, 2012).
 [2] W. Lim, B. Mayer, and T. Pawson, *Cell Signaling* (Taylor & Francis, New York, 2014).
 [3] S. Sarkar and A. E. Garcia, Presence or absence of Ras-dimerization shows distinct kinetic signature in Ras-Raf interaction, *Biophys. J.* **118**, 1799 (2020).
 [4] V. A. Ngo, S. Sarkar, C. Neale, and A. E. Garcia, How anionic lipids affect spatiotemporal properties of KRAS4B on model membranes, *J. Phys. Chem. B* **124**, 5434 (2020).
 [5] W. Bialek and S. Setayeshgar, Cooperativity, Sensitivity, and Noise in Biochemical Signaling, *Phys. Rev. Lett.* **100**, 258101 (2008).

[6] W. H. de Ronde, F. Tostevin, and P. R. ten Wolde, Effect of feedback on the fidelity of information transmission of time-varying signals, *Phys. Rev. E* **82**, 031914 (2010).
 [7] G. Tkačik and W. Bialek, Information processing in living systems, *Annu. Rev. Condens. Matter Phys.* **7**, 89 (2016).
 [8] R. Cheong, A. Rhee, C. J. Wang, I. Nemenman, and A. Levchenko, Information transduction capacity of noisy biochemical signaling networks, *Science* **334**, 354 (2011).
 [9] S. D. M. Santos, P. J. Verwee, and P. I. H. Bastiaens, Growth factor-induced MAPK network topology shapes Erk response determining PC-12 cell fate, *Nat. Cell Biol.* **9**, 324 (2007).
 [10] J. Selimkhanov, B. Taylor, J. Yao, A. Pilko, J. Albeck, A. Hoffmann, L. Tsimring, and R. Wollman, Accurate information

- transmission through dynamic biochemical signaling networks, *Science* **346**, 1370 (2014).
- [11] F. Tostevin and P. R. ten Wolde, Mutual Information between Input and Output Trajectories of Biochemical Networks, *Phys. Rev. Lett.* **102**, 218101 (2009).
- [12] N. B. Becker, A. Mugler, and P. R. ten Wolde, Optimal Prediction by Cellular Signaling Networks, *Phys. Rev. Lett.* **115**, 258103 (2015).
- [13] A. Erez, T. A. Byrd, M. Vennetilli, and A. Mugler, Cell-to-Cell Information at a Feedback-Induced Bifurcation Point, *Phys. Rev. Lett.* **125**, 048103 (2020).
- [14] G. Lan and Y. Tu, Information processing in bacteria: Memory, computation, and statistical physics: A key issues review, *Rep. Prog. Phys.* **79**, 052601 (2016).
- [15] A. Levchenko and I. Nemenman, Cellular noise and information transmission, *Curr. Opin. Biotechnol.* **28**, 156 (2014).
- [16] A. Rhee, R. Cheong, and A. Levchenko, The application of information theory to biochemical signaling systems, *Phys. Biol.* **9**, 045011 (2012).
- [17] N. Hao, B. A. Budnik, J. Gunawardena, and E. K. O'Shea, Tunable signal processing through modular control of transcription factor translocation, *Science* **339**, 460 (2013).
- [18] A. Hoffmann, A. Levchenko, M. L. Scott, and D. Baltimore, The IkappaB-NF-kappaB signaling module: Temporal control and selective gene activation, *Science* **298**, 1241 (2002).
- [19] J. E. Purvis and G. Lahav, Encoding and decoding cellular information through signaling dynamics, *Cell* **152**, 945 (2013).
- [20] K. Thurley, L. F. Wu, and S. J. Altschuler, Modeling cell-to-cell communication networks using response-time distributions, *Cell Syst.* **6**, 355 (2018).
- [21] S. Sarkar, D. Tack, and D. Ross, Sparse estimation of mutual information landscapes quantifies information transmission through cellular biochemical reaction networks, *Commun. Biol.* **3**, 203 (2020).
- [22] M. Pierobon and I. F. Akyildiz, Capacity of a diffusion-based molecular communication system with channel memory and molecular noise, *IEEE Trans. Inf. Theory* **59**, 942 (2013).
- [23] S. Kadloor, R. S. Adve, and A. W. Eckford, Molecular communication using Brownian motion with drift, *IEEE Trans. NanoBiosci.* **11**, 89 (2012).
- [24] P. B. Dieterle, J. Min, D. Irimia, and A. Amir, Dynamics of diffusive cell signaling relays, *eLife* **9**, e61771 (2020).
- [25] S. Redner, *A Guide to First-Passage Processes* (Cambridge University Press, Cambridge, 2001).
- [26] N. Hirokawa, Y. Noda, Y. Tanaka, and S. Niwa, Kinesin superfamily motor proteins and intracellular transport, *Nat. Rev. Mol. Cell Biol.* **10**, 682 (2009).
- [27] D. T. Gillespie, Exact stochastic simulation of coupled chemical reactions, *J. Phys. Chem.* **81**, 2340 (1977).
- [28] M. Z. Ali, S. Choubey, D. Das, and R. C. Brewster, Probing mechanisms of transcription elongation through cell-to-cell variability of rna polymerase, *Biophys. J.* **118**, 1769 (2020).
- [29] A. Kraskov, H. Stögbauer, and P. Grassberger, Estimating mutual information, *Phys. Rev. E* **69**, 066138 (2004).
- [30] C. M. Holmes and I. Nemenman, Estimation of mutual information for real-valued data with error bars and controlled bias, *Phys. Rev. E* **100**, 022404 (2019).
- [31] Y. Okada and N. Hirokawa, A processive single-headed motor: Kinesin superfamily protein KIF1A, *Science* **283**, 1152 (1999).
- [32] S. J. King and T. A. Schroer, Dynactin increases the processivity of the cytoplasmic dynein motor, *Nat. Cell Biol.* **2**, 20 (2000).
- [33] Z. Wang and M. P. Sheetz, The C-terminus of tubulin increases cytoplasmic dynein and kinesin processivity, *Biophys. J.* **78**, 1955 (2000).
- [34] V. Ananthanarayanan, M. Schattat, S. K. Vogel, A. Krull, N. Pavin, and I. M. Tolić-Nørrelykke, Dynein motion switches from diffusive to directed upon cortical anchoring, *Cell* **153**, 1526 (2013).
- [35] S. Klumpp, Movements of molecular motors: Diffusion and directed walks, Ph.D. thesis, University of Potsdam, 2003.
- [36] R. Grover, J. Fischer, F. W. Schwarz, W. J. Walter, P. Schuille, and S. Diez, Transport efficiency of membrane-anchored kinesin-1 motors depends on motor density and diffusivity, *Proc. Natl. Acad. Sci. USA* **113**, E7185 (2016).
- [37] J. Szymański, A. Patkowski, A. Wilk, P. Garstecki, and R. Holyst, Diffusion and viscosity in a crowded environment: From nano to macroscale, *J. Phys. Chem. B* **110**, 25593 (2006).
- [38] M. Guo, A. J. Ehrlicher, M. H. Jensen, M. Renz, J. R. Moore, R. D. Goldman, J. Lippincott-Schwartz, F. C. Mackintosh, and D. A. Weitz, Probing the stochastic, motor-driven properties of the cytoplasm using force spectrum microscopy, *Cell* **158**, 822 (2014).
- [39] F. Höfling and T. Franosch, Anomalous transport in the crowded world of biological cells, *Rep. Prog. Phys.* **76**, 046602 (2013).